Coherent Dynamics of a Single Spin Interacting with an Adjustable Spin Bath

against it. [This and further control measurements are discussed in (21).]

Much of the deviation of the data from the model can be explained by the slow drift of experimental parameters during the measurement. In particular, the observed effects are very sensitive to the focus on the sample, because the intensities of the pump, probe, and TP all vary quadratically with the focused spot size. Additional deviations may be due to the simplistic description of the TP-induced background effects used here. For example, in the case of phonon-assisted transitions to the trion state, one would expect the type of spin-selective decoherence described in (18). Although there is some finite probability for the TP to excite the trion state, the control measurements described in the supporting online text show that TP-induced spin coherence is not the dominant mechanism for the spin control observed here. Further measurements of the background effects will be needed to determine their cause, with the aim of increasing the fidelity of these single spin rotations.

In principle, at most 200 single-qubit flips could be performed within the measured T_2^* of 6 ns. However, by using shorter TPs and QDs with longer spin coherence times, this technique could be extended to perform many more operations within the coherence time. A mode-locked laser producing ~100-fs TPs could potentially exceed the threshold (~10^4 operations) needed for proposed quantum error-correction schemes (28). Additionally, the spin manipulation demonstrated here may be used to obtain a spin echo (29), possibly extending the observed spin coherence time. These results represent progress toward the implementation of scalable quantum information processing in the solid state.

References and Notes

1. A. Imamoglu et al., Phys. Rev. Lett. **83**, 4204 (1999).
2. M. Combescot, O. Betbeder-Matibet, Solid State Commun. **132**, 129 (2004).
3. P. Chen, C. Piermarocchi, L. J. Sham, D. Gammon, D. G. Steel, Phys. Rev. B **69**, 075320 (2004).
4. C. E. Pryor, M. E. Flatté, Appl. Phys. Lett. **88**, 233108 (2006).
5. S. E. Economou, L. J. Sham, Y. Wu, D. G. Steel, Phys. Rev. B **74**, 205415 (2006).
6. S. M. Clark, K.-M. C. Fu, T. D. Ladd, Y. Yamamoto, Phys. Rev. Lett. **99**, 040501 (2007).
7. F. H. L. Koppens et al., Nature **442**, 766 (2006).
8. K. C. Nowack, F. H. L. Koppens, Y. V. Nazarov, L. M. K. Vandersypen, Science **318**, 1430 (2007).
9. C. Cohen-Tannoudji, J. Dupont-Roc, Phys. Rev. A **5**, 968 (1972).
10. C. Cohen-Tannoudji, S. Reynaud, J. Phys. B **10**, 345 (1977).
11. D. Suter, H. Klepel, J. Mlynek, Phys. Rev. Lett. **67**, 2001 (1991).
12. M. Combescot, R. Combescot, Phys. Rev. Lett. **61**, 117 (1988).
13. M. Joffre, D. Hulin, A. Migus, M. Combescot, Phys. Rev. Lett. **62**, 74 (1989).
14. G. Papageorgiou et al., Phys. Rev. B **69**, 085311 (2004).
15. J. A. Gupta, R. Knobel, N. Samarth, D. D. Awschalom, Science **292**, 2458 (2001).
16. T. Unold, K. Mueller, C. Lienau, T. Elaesser, A. D. Wieck, Phys. Rev. Lett. **92**, 157401 (2004).
17. M. V. Gurudev Dutt et al., Phys. Rev. B **74**, 125306 (2006).
18. Y. Wu et al., Phys. Rev. Lett. **99**, 097402 (2007).
19. A. Greilich et al., Phys. Rev. B **75**, 233301 (2007).
20. S. G. Carter, Z. Chen, S. T. Cundiff, Phys. Rev. B **76**, 201308 (2007).
21. Supporting material is available on Science Online.
22. J. Berezovsky et al., Science **314**, 1916 (2006).
23. M. H. Mikkelsen, J. Berezovsky, N. G. Stoltz, L. A. Coldren, D. D. Awschalom, Nat. Phys. **3**, 770 (2007).
24. F. Meier, B. P. Zakharchenya, Eds., Optical Orientation: Modern Problems in Condensed Matter (North Holland, Amsterdam, 1984).
25. M. Atatüre, J. Dreiser, A. Badolato, A. Imamoglu, Nat. Phys. **3**, 101 (2007).
26. A. Von Lehmen, J. E. Zucker, J. P. Heritage, D. S. Chemla, Phys. Rev. B **35**, 6479(R) (1987).
27. D. Gammon et al., Phys. Rev. Lett. **86**, 5176 (2001).
28. D. D. Awschalom, D. Loss, N. Samarth, Eds., Semiconductor Spintronics and Quantum Computation (Springer-Verlag, Berlin, 2002).
29. M. Rosatzin, D. Suter, J. Mlynek, Phys. Rev. A **42**, 1839(R) (1990).
30. We acknowledge support from NSF and the Air Force Office of Scientific Research.

Coherent Dynamics of a Single Spin Interacting with an Adjustable Spin Bath

R. Hanson,[1]*† V. V. Dobrovitski,[2] A. E. Feiguin,[1] O. Gywat,[1] D. D. Awschalom[1]

Phase coherence is a fundamental concept in quantum mechanics. Understanding the loss of coherence is paramount for future quantum information processing. We studied the coherent dynamics of a single central spin (a nitrogen-vacancy center) coupled to a bath of spins (nitrogen impurities) in diamond. Our experiments show that both the internal interactions of the bath and the coupling between the central spin and the bath can be tuned in situ, allowing access to regimes with surprisingly different behavior. The observed dynamics are well explained by analytics and numerical simulations, leading to valuable insight into the loss of coherence in spin systems. These measurements demonstrate that spins in diamond provide an excellent test bed for models and protocols in quantum information.

Quantum systems interact with their environment, resulting in a loss of initial coherence over time (1). Such system-bath interactions are studied extensively in a few canonical examples such as the spin-boson model (2) and the central spin model. In the latter, the coherence of a single spin (the central spin) in contact with a bath of spins is investigated (3–11). Study of the central spin problem may shed light on the emergence of the classical world from a collection of interacting quantum systems (1). Moreover, understanding spin-bath interactions is crucial for using spins in solids for quantum information processing (12–14), in which the efficient isolation of single quantum systems from their environment is required.

Studies in the field of nuclear magnetic resonance (NMR) and electron spin resonance have yielded detailed information about magnetic interactions in ensembles of spins (15). Recently, it has become possible to detect and coherently control individual spins (16, 17), allowing studies of the central spin model on truly single spins and possible applications in high-resolution magnetometry (18). We report here on a detailed study of the coherent dynamics of a single spin of a nitrogen-vacancy (NV) center in contact with a bath of nitrogen (N) impurity spins in diamond.

NV centers are well suited for studying spin interactions: Their spin state can be optically imaged, initialized, and read out, as well as controlled with high fidelity. In ultrapure diamond, the spin coherence time reaches hundreds of microseconds, being limited only by the weak interactions with nuclear spins of carbon-13 (19, 20). Therefore, the presence of nearby electron spins in diamond, even if few in number, can strongly influence the NV center spin, as the magnetic moment of an electron spin is three orders of magnitude larger than that of a nuclear spin.

In type Ib diamonds, as studied here, the magnetic environment of an NV center is dominated by N impurities (21), which carry an electronic spin of 1/2. These N spins are not optically active themselves but can be detected through the magnetic dipolar coupling with the NV center spin (22, 23). Previously, spin pairs were studied in which the dynamics of a single NV center spin were dominated by a single nearby N spin (19, 24). We studied the opposite regime, where the central spin (the NV center) is

[1]California Nanosystems Institute, University of California, Santa Barbara, CA 93106, USA. [2]Ames Laboratory and Iowa State University, Ames, IA 50011, USA.

*Present address: Kavli Institute of Nanoscience Delft, Delft University of Technology, Post Office Box 5046, 2600 GA Delft, Netherlands.
†To whom correspondence should be addressed. E-mail: r.hanson@tudelft.nl

interacting with a bath of N spins. Although the spin bath extends over the whole diamond, the dynamics of each individual NV spin are mainly determined by its local environment of N spins. Therefore, the ability to image and manipulate single NV centers (16) is crucial for these studies, because variations within an ensemble can average out many of the interesting dynamics.

A NV center consists of a substitutional N atom with an adjacent vacant site (V) in the diamond lattice (Fig. 1A). Its electronic ground state is a spin triplet ($S = 1$), with an energy splitting D of 2.87 GHz between states $m_S = 0$ and $m_S = \pm 1$ due to the crystal field (m_S is the projection of the spin on the z axis) (Fig. 1B). We imaged single NV centers at room temperature using a confocal microscope (Fig. 1C). The NV spin is first optically pumped into the $m_S = 0$ sublevel (Fig. 1D). Then, pulsed radiofrequency radiation is used to coherently manipulate the spin in the dark. Finally, readout is performed by measuring the photoluminescence rate, which

reflects the spin state (16, 23). This cycle is typically repeated 10^5 times to build up statistics. The photoluminescence rate is normalized using the signal levels right after the initialization [when $p(m_S = 0) = 1$, where $p(m_S = 0)$ is the probability to be in the state $m_S = 0$] and after a π pulse [when $p(m_S = 0) = 0$].

We first showed that the spin bath properties can be controlled by subjecting the diamond to different static magnetic fields B. The total static field h_z acting on the NV center spin is the sum of B and the crystal-field splitting D (which can be viewed as an effective magnetic field) (25). We characterized the spin bath using standard NMR pulse sequences (15). We first measured the dephasing of the NV center spin during free evolution (Fig. 2A). We observe precession of the electron spin due to the hyperfine interaction with the N nuclear spin $I = 1$ of the NV center. This hyperfine shift is essentially static because of the large nuclear quadrupolar splitting and slow nuclear spin relaxation. The N spins near

the NV center create an additional field through the magnetic dipolar interactions. This bath field δh drifts with time because of N spin flips, so that the NV center experiences a different field every time a new pulse sequence is started. After averaging over many sequences, which is required to build up statistics, this drift causes rapid decay of the free evolution signal, even though δh may fluctuate only very slowly on the time scale of a single pulse sequence (that is, quasi-static dephasing). The component of δh directed along the static field h_z, δh_z, has a much larger effect than the components perpendicular to h_z (such as δh_x and δh_y). This can be seen by transforming to the rotating frame of the spin (Fig. 2B). Here δh_x and δh_y are averaged out by fast rotations around h_z, whereas δh_z is unaffected by the transformation. The damping of the free evolution has a Gaussian shape, indicating that the distribution of δh_z, $P(\delta h_z)$, is also Gaussian: $P(\delta h_z) = 1/\sqrt{2\pi b^2} \exp(-\delta h_z^2/2b^2)$ (15). Its standard deviation b can be extracted from the decay during free evolution (25). Values for b are in the range of 0.3 to 1.1 MHz for four NV centers investigated, which is in good agreement with the average separation between N spins in this diamond of a few nanometers.

The static dephasing can be canceled with a spin echo (Fig. 2C). The time scale T_2 on which the spin echo signal decays (the spin coherence time) is proportional to the fluctuation rate of the spin bath (15). T_2 is almost an order of magnitude longer at $B = 740$ G than at $B = 0$ G, revealing a drastic change in the bath dynamics upon application of a magnetic field. This is explained by the dependence of the energy levels on the magnetic field (Fig. 2D). Close to $B = 0$ G, the average dipolar coupling between the N spins is larger than the energy splitting between the spin states, causing rapid fluctuations in the spin orientations (Fig. 2E). An applied magnetic field

Fig. 1. Detection and manipulation of a single spin. (**A**) Structure of an NV center in the diamond lattice. (**B**) The level structure of the NV center. The NV center is optically excited with a laser at 532 nm. Photoluminescence (PL) is measured with a confocal microscope. (**C**) Spatial PL map of part of the diamond sample, showing bright spots corresponding to single NV centers. (**D**) Measurement cycle consisting of initialization for 3 μs, manipulation through rf radiation that rotates the spin with Rabi frequencies of 5 to 30 MHz, and readout for 2 μs.
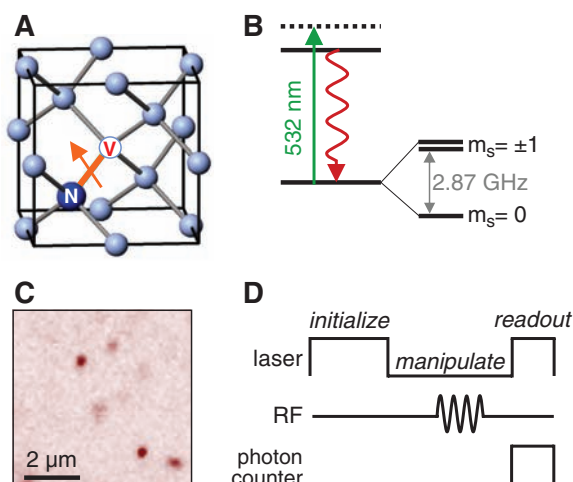

Fig. 2. Characterization of the spin bath. (**A**) Measurement of dephasing during free evolution of NV14. The Ramsey pulse scheme used is π/2-τ-π/2, where τ is the free evolution time. At $B = 0$ G, a superposition of $m_S = 1$ and $m_S = -1$ is prepared, whereas at $B = 740$ G, a superposition of $m_S = -1$ and $m_S = 0$ is prepared, resulting in opposite values at $\tau = 0$ (24). Fitting to a Gaussian envelope decay yields $b = (0.42 \pm 0.03)$ MHz at $B = 0$ G and $b = (1.09 \pm 0.15)$ MHz at $B = 740$ G. (**B**) Bloch sphere representation of dephasing due to fluctuations δh of the total magnetic field h_z. In the rotating frame of the spin, only fluctuations along the magnetic field; that is, δh_z; are significant. (**C**) Measurement of T_2 of NV14 using a π/2-τ-π-τ-π/2 spin echo pulse scheme. Fitting to exp($-2\tau/T_2$) yields $T_2 = (0.39 \pm 0.04)$ μs at $B = 0$ G and $T_2 = (3.2 \pm 0.4)$ μs at $B = 740$ G. (**D**) Energy of a single N electron spin (top) and a single NV center electron spin (bottom) as a function of B. (**E**) Schematic of the spin-bath dynamics at $B = 0$ G and $B = 740$ G.
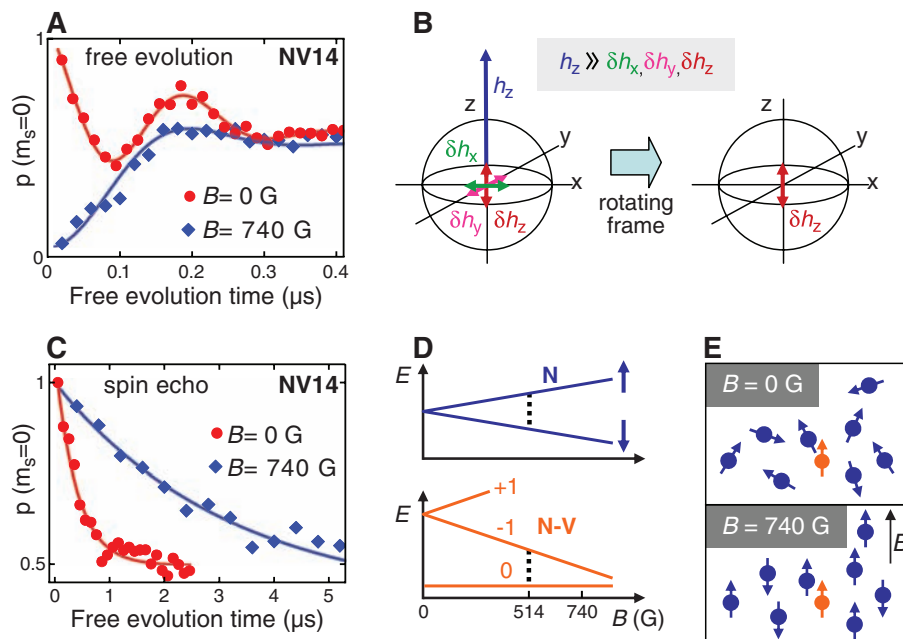
induces a large Zeeman energy splitting, which freezes out most of the spin dynamics (25). These experiments demonstrate that by tuning the magnetic field, we can control the dynamics within the spin bath.

We studied the spin-bath dynamics in more detail by measuring coherently driven spin oscillations (Rabi oscillations) at different magnetic fields. At $B = 0$ G (Fig. 3A), the oscillations initially decay fast and collapse almost completely, revive, and finally damp out slowly. This com-

plex behavior is reproduced at other NV centers and is observed for different driving fields.

To gain insight into these dynamics, we used analytical calculations and numerical simulations, based on existing knowledge about the internal structure of NV centers and N impurities (26). The dynamics of the NV spin were simulated numerically, using six N impurities at random locations, with the local density of N impurities being the only unknown parameter. This density was adjusted to match the data from the Ramsey

measurement (25). We explicitly take the nuclear spins of the nitrogen impurities into account, so that every impurity is, in fact, a system of two coupled spins (the electron with spin $S = 1/2$ and the nucleus with $I = 1$). Also, an analytical description was constructed by modeling the spin bath as a random field acting on the NV spin (25, 27, 28). The static and dynamical components of this field are characterized by the parameters b and T_2, respectively, whose values are known from the Ramsey and spin echo measure-

Fig. 3. Rabi oscillations at 0 G. (**A**) (Top) Rabi oscillations of NV14 at $B = 0$ G. (Middle) Analytical calculation of Rabi oscillations at $B = 0$ G for $b = 0.42$ MHz and a driving frequency of 16.6 MHz. (Bottom) Numerical simulation of Rabi oscillations at $B = 0$ G using a bath of six N spins. (**B**) (Left) Depiction of the magnetic fields in the rotating frame for the case of Rabi oscillations driven by an on-resonance field h_x. (Right top) Gaussian distribution of magnetic fields along z in the rotating frame with $b = 0.45$ MHz. (Right bottom) Rabi oscillations of a two-level system for $h_x = 8$ MHz, numerically averaged over the field distribution from the right top panel. (**C**) Same as (B), but with a static offset Δh_z of 2.3 MHz along z.
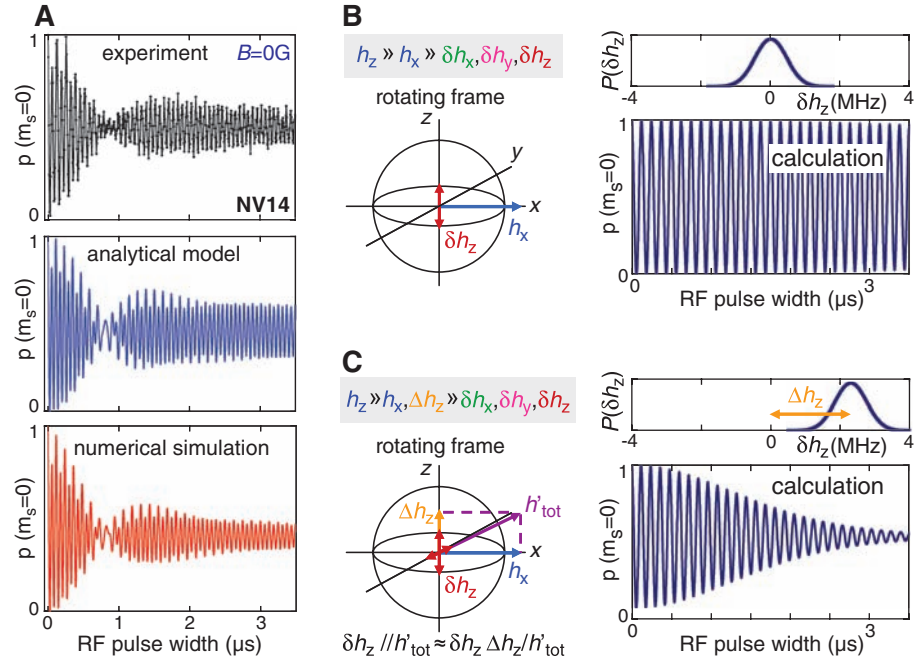

Fig. 4. Rabi oscillations at 740 and 514 G. (**A**) Rabi oscillations of NV14 at $B = 740$ G. (**B**) Distribution of fields along z in the rotating frame, for $b = 1.1$ MHz and $\Delta h_z = 0, \pm 2.3$ MHz. The thick blue line is the sum of the three distributions. (**C**) Rabi oscillations of a two-level system for $h_x = 10$ MHz, numerically averaged over the total field distribution in (B). (**D**) Rabi oscillations of NV14 and (**E**) NV31 at $B = 514$ G. Red lines are fits to an exponentially damped sum of two cosines with different frequencies. (**F**) Fast Fourier transforms (FFT) of curves in (D) (left) and (E) (right), revealing two dominant nutation frequencies. Ampl., amplitude; arb., arbitrary. (**G**) Plot of the lower nutation frequency versus the higher nutation frequency derived from Rabi oscillations at $B = 499$ G (triangles), $B = 514$ G (circles), and $B = 530$ G (squares). Different colors correspond to different NV centers. The gray line highlights the universal proportionality factor of $\sqrt{2}$.
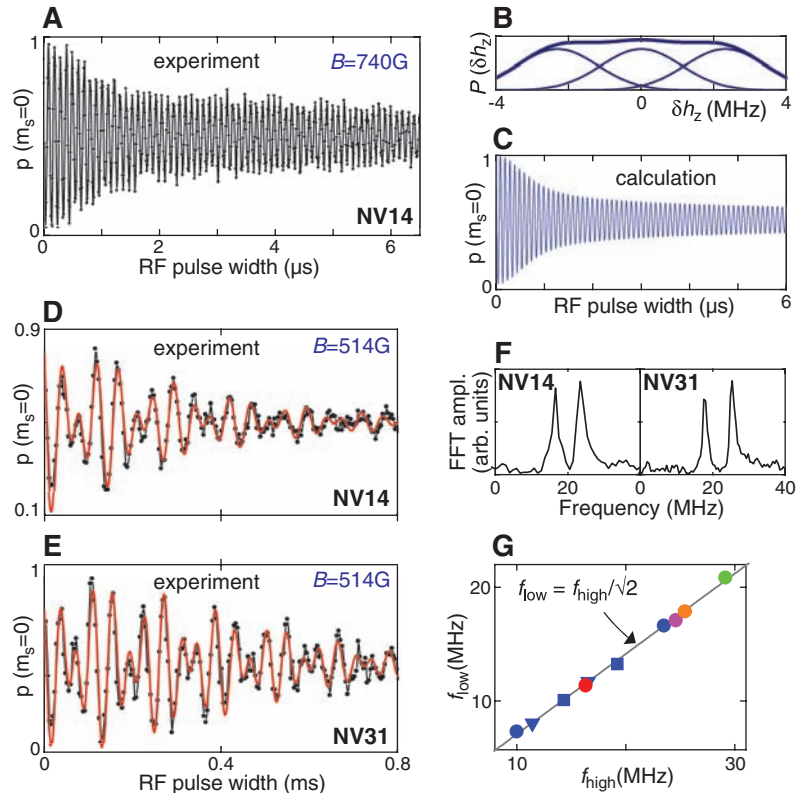
ments. For the Rabi oscillations, the dynamical component is neglected in the analytical model. Both the analytics and the numerical simulations accurately reproduce the essential features of the Rabi oscillations at $B = 0$ G without any fitting parameters (Fig. 3A): collapse and revival of the amplitude, beating of the oscillations at short times, and slow power-law decay after the revival.

From the theoretical analysis we find that the N nuclear spin of the NV center plays an essential role in the observed dynamics. Figure 3B depicts the fields acting on the spin in the frame rotating at frequency h_z, in case the nuclear spin is in the $m_I = 0$ state. Besides the fluctuating bath field δh_z, there is a strong driving field h_x, which rotates at the Larmor frequency set by h_z and thus appears static in the rotating frame. This case is equivalent to that shown in Fig. 2B, with h_z replaced by h_x and δh_x replaced by δh_z. Because δh_z is perpendicular to h_x, it is averaged out by fast spin precession around h_x and therefore has a very small effect on the dynamics: Rabi oscillations in this case show a slow power-law decay (4, 9, 10). In contrast, if the nuclear spin is in the $m_I = \pm1$ state (Fig. 3C), a large static offset Δh_z results because of the hyperfine interaction that tilts the sum of the fields, h'_{tot}, toward the z axis. In this case, the bath field δh_z has a component parallel to the total field h'_{tot}. This component is not affected by the fast precession around h'_{tot}. Again there is a correspondence with Fig. 2B, but now δh_z is replaced by $\delta h_z(\Delta h_z/h'_{tot})$. Although the distribution of the bath field is the same as in Fig. 3B, the Rabi oscillations decay rapidly with a Gaussian envelope because of the component parallel to h'_{tot}.

Experimentally, we measured the average over the nuclear spin configurations. The spin nutation (Rabi) frequency in the case of $m_I = \pm1$ is slightly larger than in the case of $m_I = 0$, by a factor $\sqrt{(h_x^2 + \Delta h_z^2)}/h_x$. Therefore, beating will occur upon averaging because of interference between the oscillations corresponding to $m_I = 0$ and $m_I = \pm1$, resulting in repeated collapse and revival. Because the oscillations corresponding to $m_I = \pm1$ die out rapidly, only a single collapse and revival are visible. After the revival, the remaining signal is completely due to the $m_I = 0$ oscillations.

Even though the spin echo experiment indicates that the bath already changes on a time scale of 0.4 μs, our analytical model assuming a static bath shows excellent agreement with the data. The reason for this robustness is that under continuous driving, the spin is insensitive to fluctuations with a frequency below the Rabi frequency.

At $B = 740$ G, the collapse and revival are not observed in the Rabi oscillations (Fig. 4A). Because of alignment of the spins along B, the width of the bath field distribution is different than at $B = 0$ (25). For the measured value for b of 1.1 MHz, the distributions for the three possible NV nuclear spin states strongly overlap (Fig. 4B). As a consequence, the interference between the distributions leading to collapse is absent (Fig. 4C). Instead, the oscillations corresponding to the ex-

treme values of δh_z decay fast, and those corresponding to the more central values lead to a slow $1/\sqrt{t_{pw}}$ decay [t_{pw} is the radio frequency (rf) pulse width] (4, 9, 10).

The central spin and the bath spins can be brought into energy resonance by applying a magnetic field that exactly compensates for the NV center's crystal field splitting (near $B = 514$ G, Fig. 2D) (22, 23, 29). Here, the N electron spins can exchange their spins resonantly with the central spin through mutual flip-flops, providing an additional, efficient path for decoherence. Moreover, at this magnetic field the N spins are also resonant with the driving field and therefore will undergo driven rotations.

Figure 4, D to E, show Rabi oscillations at $B = 514$ G for two different NV centers. The oscillations clearly decay much faster than at $B = 740$ G. Furthermore, the data can be well fit to an exponential decay, as opposed to the power-law decay that was observed at $B = 740$ G. These observations suggest that in this regime the resonant spin flip-flop mechanism indeed dominates the decay of the Rabi oscillations.

A closer look at the data in Fig. 4, D to E, reveals a pronounced beating pattern. From a Fourier analysis (Fig. 4F) we find that there are two dominant oscillation frequencies. In Fig. 4G we plot the lower of these two frequencies, f_{low}, versus the higher frequency, f_{high}, for different NV centers and for different experimental conditions. The two frequencies differ exactly by a factor of $\sqrt{2}$, for all five NV centers investigated and for all driving frequencies.

Because of the strong hyperfine interaction of the N electron spin with its nuclear spin (26), the resonance condition also occurs at $B = 499$ G and $B = 530$ G (22, 23). We observe the same beating pattern at these fields. At $B = 522$ G, where the central spin and the bath are not resonant, only the higher of the two oscillation frequencies is present. This indicates that the lower oscillation frequency is induced by the resonance condition.

For a spin of $S = 1$ (as the NV center has), the Rabi frequency is larger than for a spin of $S = 1/2$ (as the N spins have) for the same driving field by $\sqrt{2}$ (15, 25). Therefore, the observed factor of $\sqrt{2}$ strongly suggests that the coherent rotation of N spins is the cause of the beating pattern. Rotation of the N spins will cause the dipolar field at the NV center to oscillate with f_{low}, which could in turn rotate the NV spin. However, the beating pattern is not reproduced by simulations or analytics if equilibrium conditions are assumed, suggesting that strongly nonequilibrium effects such as a polarization of the spin bath and initial entanglement between the central spin and the bath may play a crucial role. More work is needed to investigate this.

The use of more complicated pulse sequences will allow new studies of fundamental quantum-mechanical models and tests of protocols for future quantum information-processing tasks. Moreover, this system can be used as a test bed for similar systems, such as an electron spin cou-

pled to a bath of nuclear spins in a quantum dot (17), which lack the tunability and level of coherent control demonstrated here. Finally, the spin baths in our sample were formed randomly during crystal growth. Using the recently gained ability to position single spins in diamond by ion implanting (30), spin environments may soon be studied that are engineered from scratch.

References and Notes

1. W. H. Zurek, *Rev. Mod. Phys.* **75**, 715 (2003).
2. A. J. Leggett *et al.*, *Rev. Mod. Phys.* **59**, 1 (1987).
3. N. V. Prokof'ev, P. C. E. Stamp, *Rep. Prog. Phys.* **63**, 669 (2000).
4. V. V. Dobrovitski, H. A. De Raedt, M. I. Katsnelson, B. N. Harmon, http://arxiv.org/abs/quant-ph/0112053 (2001).
5. A. V. Khaetskii, D. Loss, L. Glazman, *Phys. Rev. Lett.* **88**, 186802 (2002).
6. I. A. Merkulov, A. L. Efros, M. Rosen, *Phys. Rev. B* **65**, 205309 (2002).
7. R. de Sousa, S. Das Sarma, *Phys. Rev. B* **68**, 115322 (2003).
8. V. V. Dobrovitski, H. A. De Raedt, M. I. Katsnelson, B. N. Harmon, *Phys. Rev. Lett.* **90**, 210401 (2003).
9. F. M. Cucchietti, J. P. Paz, W. H. Zurek, *Phys. Rev. A* **72**, 052113 (2005).
10. J. M. Taylor, M. D. Lukin, *Quant. Info. Process.* **5**, 503 (2006).
11. W. Yao, R.-B. Liu, L. J. Sham, *Phys. Rev. Lett.* **98**, 077602 (2007).
12. D. Loss, D. P. DiVincenzo, *Phys. Rev. A* **57**, 120 (1998).
13. B. E. Kane, *Nature* **393**, 133 (1998).
14. D. D. Awschalom, D. Loss, N. Samarth, Eds., *Semiconductor Spintronics and Quantum Computation* (Springer, Berlin, 2002).
15. C. P. Slichter, *Principles of Magnetic Resonance* (Springer-Verlag, New York, 1990).
16. F. Jelezko, T. Gaebel, I. Popa, A. Gruber, J. Wrachtrup, *Phys. Rev. Lett.* **92**, 076401 (2004).
17. R. Hanson, L. P. Kouwenhoven, J. R. Petta, S. Tarucha, L. M. K. Vandersypen, *Rev. Mod. Phys.* **79**, 1217 (2007).
18. B. M. Chernobrod, G. P. Berman, *J. Appl. Phys.* **97**, 014903 (2005).
19. T. Gaebel *et al.*, *Nat. Phys.* **2**, 408 (2006).
20. L. Childress *et al.*, *Science* **314**, 281 (2006).
21. T. A. Kennedy, J. S. Colton, J. E. Butler, R. C. Linares, P. J. Doering, *Appl. Phys. Lett.* **83**, 4190 (2003).
22. E. van Oort, P. Stroomer, M. Glasbeek, *Phys. Rev. B* **42**, 8605 (1990).
23. R. J. Epstein, F. M. Mendoza, Y. K. Kato, D. D. Awschalom, *Nat. Phys.* **1**, 94 (2005).
24. R. Hanson, F. Mendoza, R. J. Epstein, D. D. Awschalom, *Phys. Rev. Lett.* **97**, 087601 (2006).
25. See supporting material on *Science* Online.
26. J. H. N. Loubser, J. A. van Wyk, *Rep. Prog. Phys.* **41**, 1201 (1978).
27. G. M. Zhidomirov, K. M. Salikhov, *Sov. Phys. J. Exp. Theor. Phys.* **29**, 1037 (1969).
28. J. R. Klauder, P. W. Anderson, *Phys. Rev.* **125**, 912 (1962).
29. R. Hanson, O. Gywat, D. D. Awschalom, *Phys. Rev. B* **74**, 161203(R) (2006).
30. J. R. Rabeau *et al.*, *Appl. Phys. Lett.* **88**, 023113 (2006).
31. We acknowledge support from the Air Force Office of Scientific Research and the Dutch Organization for Fundamental Research on Matter (FOM). A.E.F is a member of Microsoft Station Q and acknowledges support from the Microsoft Corporation. Work at the Ames Laboratory is supported by the U.S. Department of Energy, Basic Energy Sciences, under contract DE-AC02-07CH11358.